Solids Transport Modeling in a Fluidized Drum Granulator†

Rodrigo Rojas, Juliana Piña,* and Verónica Bucalá

Department of Chemical Engineering, Universidad Nacional del Sur, PLAPIQUI, CONICET, Camino La Carrindanga Km. 7, (8000) Bahía Blanca, Argentina

The fluidized-bed granulator (FDG) involves the use of a fluidized bed in a drum granulator, which is a horizontal cylinder fitted with internal flights. Despite its demonstrated success on an industrial scale, there are few published fundamental studies of this granulation process. In this work, a mathematical model to represent the solids flow pattern within the different active and passive zones of the rotating FDGs is developed. The fluidization table geometry as well as the angular velocity, drum inclination angle, and flights number strongly affect the mass holdups. Relatively high rotational speeds, inclination angles, and number of flights allow increasing the active mass holdups, reducing the passive mass, and eliminating the kilning flow. The model presented in this work, which accounts for the solids mass flows and holdups in the different zones of a FDG, provides a firm foundation for integration with energy and population balances.

1. Introduction

Granulation is an important particle size enlargement process, widely used in the pharmaceutical, agricultural, fertilizer, and mining industries. Granulation includes a number of processes that purposely convert, by a sequence of events, small particles into large permanent masses in which the initial primary units are still identifiable. Several granulation technologies are used for particles growth with different aims, such as improving handling and flowability, obtaining a certain size, enhancing the product appearance, controlling the particle moisture content, reducing dusting or material losses, producing structurally useful forms, etc.[1−3]

The granulation of solid particles implies two joint conditions: primarily, particles must be thoroughly mixed, and second, the binder must be applied to the moving bed of particles in the appropriate manner and form. Particularly, the wet or melt granulation employs a liquid as a binder to promote the particles enlargement. The powder mixing can be performed either mechanically (e.g., higher shear mixers, rotating drums, and pans) or pneumatically, as occurs in the fluidized beds.[4]

Kaltenbach-Thuring S.A. developed the fluidized-bed drum granulation process for granulating various inorganic fertilizers. This technology began to be used in the industry in 1986.[5] The fluidized-bed granulator (FDG) consists of the combination of a drum granulator and a fluidized bed installed inside the unit. It is claimed that the main advantages of this process are, among others, its universal character, which allows using this technology to granulate any type of product provided it can be molten, dissolved, or suspended in the form of a pumpable liquid or slurry; its simplicity; the production of very high quality granules; and the possibility to use it also for particles (prills or granules) fattening/coating.[6,7]

Figure 1 shows the FDG scheme given by Lauchard and Kordek.[7] The FDG is an inclined (from the horizontal) cylinder fitted with internal flights. The drum rotates around its axis, and a fluidized bed is located within it where air is blown upward. The fluidization table is also inclined to allow the solids discharge toward the drum bottom. This design offers the very good heat and mass transfer rates provided by fluidization but with lower air flow rates than the fluidized-bed granulators.[6,8]

The FDG modeling is quite complex; the mathematical description of the particles circulation pattern is one of the main difficulties. As is shown in Figure 2, the granules inside the unit are mechanically raised by the flights, sliding and rolling, up to the upper part of the drum, from where they fall onto the fluidized bed for cooling or drying (i.e., melt or wet granulation, respectively). The slope of the fluidized table surface allows the particles to flow down along the inclined perforated plate and fall into the lower part of the drum after being sprayed with the liquid binder. The flights raise the granules coated with a new layer to be further cooled or dried. The same cycle is then repeated until the desired particle size is achieved.[9]

Despite its demonstrated success on an industrial scale, there are few published fundamental studies of this granulation

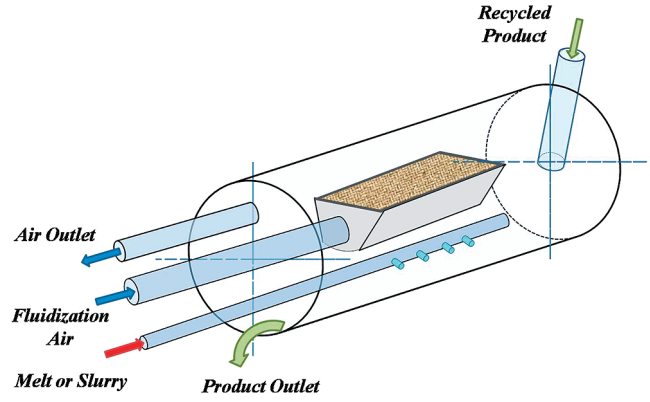

Figure 1. Fluidized drum granulator (from ref 7).

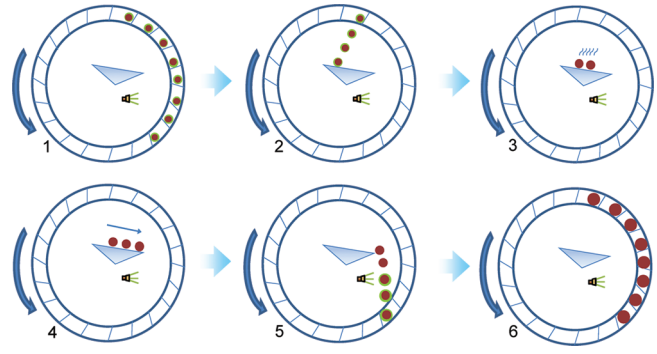

Figure 2. Solids transport within the FDG.

† Part of the Special Issue to honor Professor Hugo de Lasa.

* To whom correspondence should be addressed. Tel.: 54-291-486-1700, ext. 265. Fax: 54-291-486-1600. E-mail: julianap@plapiqui.edu.ar.

10.1021/ie901691v
Published on Web 02/08/2010

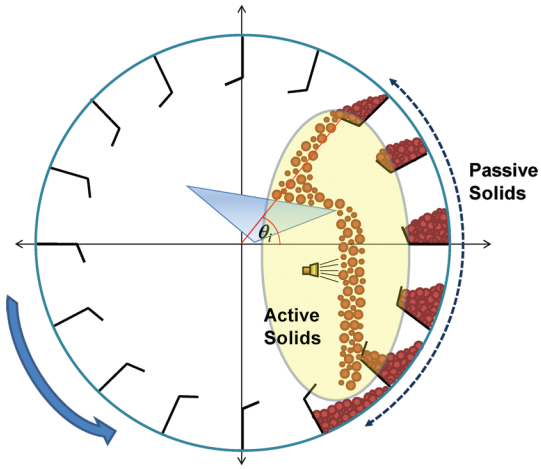

Figure 3. Active and passive solids within the FDG.

process.[10,11] To the best of our knowledge, there is a lack of research papers involving the design and modeling of FDGs with the purpose of understanding and improving their operation. Contrarily, there is abundant literature regarding mathematical models to represent the solids flow pattern within rotating drum dryers with internal flights.[12−18]

In this work, some previous studies by other authors about drum dryers are extended to represent the solids movement within a fluidized drum unit to carry out a melt granulation process for fertilizer production. The developed model is used for design purposes (i.e., the definition of the drum dimensions, the inclination and rotational speed, the geometry and number of flights, and the fluidized-bed table dimensions and location within the drum). The effect of the design parameters on the solids holdup and operating regime is analyzed.

2. Mathematical Model

For flighted rotary dryers, many authors, among others Sheehan et al.[16] and Britton et al.,[17] proposed a solids transport compartment model involving perfectly mixed tanks linked in a series arrangement. Each cell or compartment exchanges mass with the subsequent one. For a FDG, this model is an attractive basis to work with; however, the phenomena that occur on the fluidization table (cooling/solvent evaporation) and within the binder spray zone should also be considered.

Several authors agree to classify the solids, within a cell, in two discrete phases according to where they are located in the unit.[13,17,19] One phase represents the material contained in the flights and in the bottom of the drum (passive phase), while the other phase represents the solids falling toward the drum bottom (active phase). Figure 3 shows the active and passive solids in a fluidized drum granulator; the solids on the fluidization table belong to the named active zone.

In a FDG, the active and passive zones are exchanging mass continuously with a rate that depends on the solid properties and the granulator operating conditions. The mass exchange is due to the solids transport in the axial and transversal directions.[10,18]

2.1. Axial Solids Transport. The active and passive solids exhibit a mass transport along the FDG axial axis. As can be seen in Figure 4, the active particles discharged from the flights are displaced in the axial direction mainly due to the drum inclination angle (α_d).

Ideally, flighted rotating drums would operate under design-loaded conditions, where the flights entering the upper half of

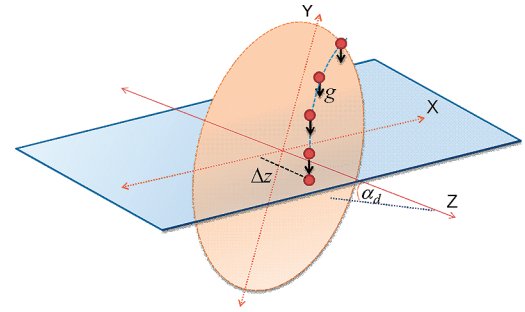

Figure 4. Axial motion of falling particles.

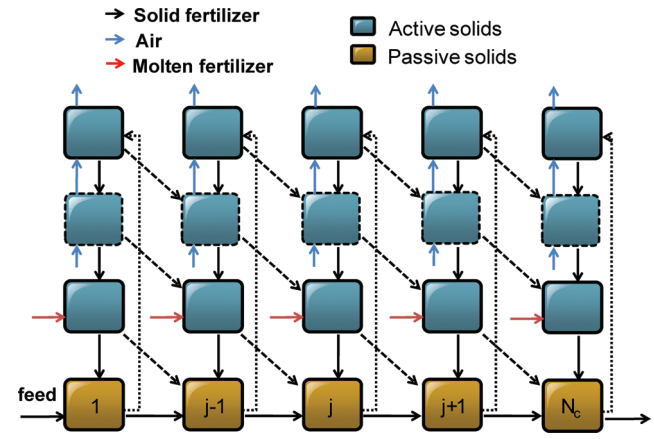

Figure 5. Solids transport within the FDG between active and passive phases and different cells.

the drum contain the maximum allowable amount of solids. However, in practice, these units are usually either underloaded (where there are insufficient solids to completely fill the flights) or overloaded (where there is more solids than the flights can carry). When the drum is overloaded, the solids in excess that remain in the bottom of the drum are also axially transported along successive passive tanks with a flow rate known as kilning flow.

2.2. Solids Transversal Transport. The solids transport in the FDG transversal direction, caused by the flight mass transport and the drum rotation, can be considered to occur in four stages:

• Step 1: The solids transported by the flights are discharged as a curtain onto the fluidization table.

• Step 2: Because of the fluidization table inclination, the particles roll down along its length.

• Step 3: The solids fall down through the spray zone, from the fluidization table edge to the drum bottom.

• Step 4: The particles are lifted to the upper half part of the drum to start step 1 again.

2.3. Cells Model for the FDG Representation. On the basis of the compartments model reported in the open literature for rotary drum driers[16−18] and the FDG distinctive features, Figure 5 shows a scheme of the cells model proposed for the FDG. This model structure, which considers the existence of a fluidization table in the middle of the active region and a spraying bar fitted with numerous two-fluid nozzles below the table edge axially equispaced, allows the representation of the four stages described previously for the transversal transport of the solids.

As can be seen in Figure 6 for a typical *j*th cell, the solids, air (used for cooling purposes in melt granulation), and binder are transported into and/or out of these subcells in a number of

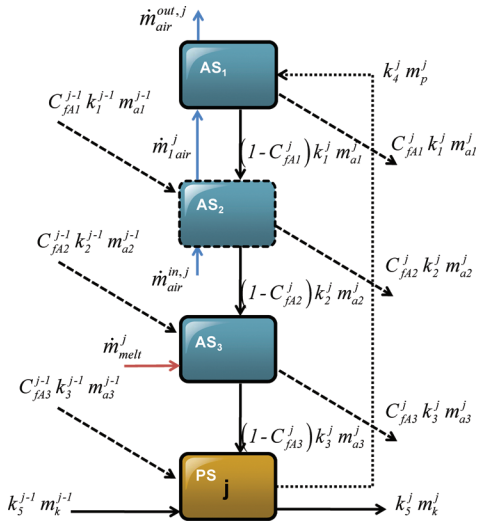

Figure 6. Mass flows in and out of the *j*th cell.

ways, with the solids motion being both between phases within the same cell and toward neighboring compartments.

According to previous researchers,[16,18] the solids transport out of a subcell is proportional to the mass contained in it. In other words, the mass flow of solids leaving each subcell can be expressed as

$$\dot{m} = km \tag{1}$$

where $\dot{m}$ and m are the mass flow rate and holdup of the subcell, respectively. The solids transport coefficient k is related to the inverse of the solids residence time in a given subcell.

In Figure 6 and according to eq 1, $k_4^j m_p^j$ represents the mass flow rate of the solids that are transported out of the passive phase through discharge from the flights into the active solids above the fluidization table (AS1), with m_p^j being the solids mass belonging to the passive phase of cell j. Because of the FDG slope, this mass flow can either fall in the active zone AS1 of the same cell or forward. For this reason, the total stream leaving the active zone AS1 ($k_1^j m_{a1}^j$) is split between two flows: $C_{fA1}^j k_1^j m_{a1}^j$, which represents the active solids fraction in the fluidization bed that is discharged to the contiguous cell, and $(1 - C_{fA1}^j)\, k_1^j m_{a1}^j$, which is the fraction of solids that falls in the same compartment. C_{fA1}^j is defined as the forward partitioning coefficient for the zone AS1.

To avoid the undesired granules agglomeration, most of the solids discharged from the flights should reach the fluidization table to be cooled down. The granules that fall down from the fluidization table edge should be at a temperature low enough to allow the solidification of the sprayed molten binder before the solids reach the drum bottom. In fact, the FDG design should guarantee that all the material transported by the flights is discharged onto the fluidization table before falling through the spraying zone or toward the drum bottom.[11] Therefore, it is assumed that all the solids transported by the flights fall within the fluidization area. The particles that fall down from the table edge can either pass through the spray zone of the same cell ($(1 - C_{fA2}^j)\, k_2^j m_{a2}^j$ or the contiguous one ($C_{fA2}^j k_2^j m_{a2}^j$). As a final step within the active zone, the solids that have been coated by binder drops can be either discharged in the passive cells j[$(1 - C_{fA3}^j)\, k_2^j m_{a3}^j$] or ($j + 1$)($C_{fA3}^j k_3^j m_{a3}^j$).

The drum design load is a critical parameter to identify the existence or not of the kilning flow. Porter[20] simply suggested that the design load is equal to the amount of passive solids required to entirely fill one-half of the flights within the drum.

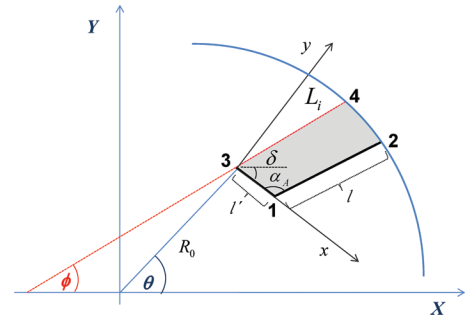

Figure 7. Flight in a FDG with its tip at the rotation angle θ.

Thus,

$$m_{p,design}^j = \frac{N_f}{2} m_{f,i=1}^j \tag{2}$$

where for a cell j, $m_{p,design}^j$ is the design load, N_f is the flights number, and $m_{f,i=1}^j$ is the maximum load of a flight ($i = 1$ or $\theta_i = 0$). According to Porter,[20] a flight is filled to maximum load when its tip is located at the horizontal position (see Figure 7 for $\theta_i = 0$).

If the passive solids mass in any cell exceeds the design point, the kilning flow appears between the passive phase of successive cells, and the flights operate at their maximum capacity. Therefore, the flow of solids transported by the flights up to the active subcell AS1 reaches a maximum value: $|k_4^j m_p^j|_{max}$. Consequently, if the FDG is operated at overloaded conditions, the following flow rates should be considered:[16,17]

$$|k_4^j m_p^j|_{max} = k_4^j m_{p,design}^j \tag{3}$$

$$\dot{m}_k^j = k_5^j (m_p^j - m_{p,design}^j) = k_5^j m_k^j \tag{4}$$

2.4. Flight Holdup and Discharge Flows. To estimate the transport coefficients and then solve the cells mass balances of the system presented in Figure 6, an estimation of the mass flows of the solids discharged from the flights as the drum rotates are required. With this aim, in this section, the flight holdup is first derived.

Figure 7 shows a flight in a FDG with its tip located at the rotational angle θ with respect to the horizontal centerline. The angle is measured in the direction of rotation, which is counterclockwise.[15] The rotational angle θ can be related with the number of flights and the discharge angular position (i) as follows:[17]

$$\theta_i = (i - 1)\frac{2\pi}{N_f} \quad i = 1, ..., \frac{N_f}{2} + 1 \tag{5}$$

Equation 5 places θ between 0 and π, because the flights discharge solids in the upper half of the drum.[17] As the drum rotates, a flight will collect or discharge material depending on its angular location θ and the drum loading.

For each cell, the flight load is calculated as follows:

$$m_{f,i}^j = S(\theta_i)\rho_b \frac{L_f}{N_c} \tag{6}$$

where $S(\theta_i)$ is the cross-sectional area occupied by the solids in the flight at the angular position θ_i; L_f represents the drum length, which is assumed to be equal to the flight length; ρ_b is the solids bulk density; and N_c denotes the number of compartments selected for the FDG cells model.

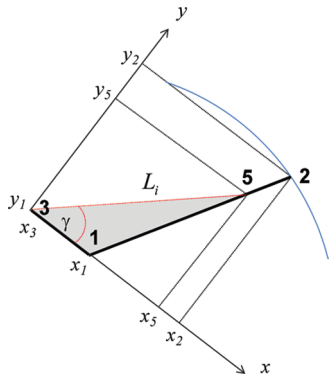

Figure 8. Flight cross-sectional area when the particles do not reach the drum wall but contact the base segment.

To evaluate the flight cross-sectional area for two-segment perpendicular flights (as the one shown in Figure 7), the procedure proposed by Lisboa et al.[21] is applied.

The kinetic angle of repose (ϕ), shown in Figure 7, is the angle of the level of the free-flowing particles to the horizontal.[13] Since for melt granulation the granules can be assumed to be completely solidified when they are lifted up by the flights[11] and the particles do not change their sizes dramatically during the enlargement process, a constant kinetic repose angle along the axial direction of the FDG is considered.

As suggested by Lisboa et al.,[21] to establish the location of a flight in the FDG, the following two-axes systems are required: (a) a fixed coordinate system located at the drum center (X, Y) and (b) a moving coordinate system placed at the tip of the flight (x, y). The flight cross-sectional area can be determined if the coordinates of the intersection of the solids surface with the segments of the flights or the drum wall are known.

As proposed by Lisboa et al.,[21] for flights sufficiently separated to avoid interference effects, the three following flight loading cases are considered:

(i). The solids held in the flight contact the drum wall (see Figure 7). Given $\gamma = \phi - \delta$, the particles reach the drum wall if $\gamma > \arctan((y_2)/(x_2))$. In this case, the sectional area is calculated as

$$S(\theta_i) = \frac{R^2}{2}[\beta - \sin(\beta)] + \frac{1}{2}\left|y_2x_1 + y_4x_2 - y_2x_4\right| \quad (7)$$

where the parameter β is defined as follows:

$$\beta = \arcsin\left[\frac{[(x_2 - x_4)^2 + (y_2 - y_4)^2]^{1/2}}{2R}\right] \quad (8)$$

For $\theta_i = 0$, eq 7 leads to the maximum allowable cross-sectional area occupied by the solids in the flight. This condition is used to establish the FDG load regime and the mass flow rates discharged by the flights, which affect the mass-average cycle time and thus the transport coefficients.

(ii). The solids held in the flight contact the base segment of the flight but do not reach the drum wall (see Figure 8). This situation takes place when: $\gamma < \arctan((y_2)/(x_2))$, $[(x_5 - x_1)^2 + (y_5 - y_1)^2]^{1/2} < l'$, and $y_5 > 0$. The cross-sectional area is given by the surface of the triangle $1\hat{3}5$:

$$S(\theta_i) = \frac{1}{2}|x_1y_5| \quad (9)$$

where y_5 is the ordinate value of the intersection between the solids level and the flight base segment.

(iii). The flight is empty. The flight becomes empty when $y_5 = 0$. Obviously the cross-sectional area results as follows:

$$S(\theta_i) = 0 \quad (10)$$

The dynamic angle of repose ϕ_i as a function of the flight angular position θ_i is calculated as suggested by Schofield and Glikin:[22]

$$\tan(\phi_i) = \frac{\mu + R_0\frac{\omega^2}{g}[\cos(\theta_i) - \mu\sin(\theta_i)]}{\mu - R_0\frac{\omega^2}{g}[\sin(\theta_i) - \mu\cos(\theta_i)]} \quad (11)$$

where R_0 is the distance from the flight tip to the center of the drum and μ is a property of the solids called the dynamic coefficient of friction. For several fertilizers, this coefficient lies between the values 0.2 and 0.6.[23−25]

By estimation of the cross-sectional area of the solids contained in a flight, the flight mass holdup for each cell and angular position can be calculated through eq 6. As proposed by Britton et al.,[17] to determine the drum load regime (i.e., the existence or not of kilning flow), the distribution of passive solids between the discharging flights (flight-passive solids) and the drum bottom (drum-passive solids) is required. Considering eqs 2 and 6, the mass holdup of the drum-passive solids is calculated as follows:

$$m^j_{\mathrm{p,drum}} = m^j_{\mathrm{p,design}} - \sum_i m^j_{\mathrm{f},i} \quad (12)$$

To evaluate the transport coefficients, which are related to the solids cycle times in different zones of the FDG, an estimation of the mass flows of the solids discharged from the flights as the drum rotates has to be calculated. According to Sherritt et al.[13] and Britton et al.,[17] the instantaneous discharged mass flows are calculated as follows:

$$-\frac{\mathrm{d}m^j_{\mathrm{f},i}}{\mathrm{d}t} = \dot{m}^j_{i_{\mathrm{A1}}} = \rho_{\mathrm{b}}\omega\frac{L_{\mathrm{f}}}{N_{\mathrm{c}}}\frac{L_i^2}{2} \quad (13)$$

where ω is the angular velocity and L_i is the length of surface cord on a discharging flight (see Figures 7 and 8). Equation 13 has to be computed when the relationship $\phi_i < \theta_i$ is satisfied.

2.5. Solids Transport Coefficients. To completely solve the model, the solids transport coefficients have to be calculated. These parameters can be established if the active and passive cycle times are first computed.[17] The existence of the fluidization table and spray nozzle within the drum requires a new method, which is proposed in this paper, to evaluate the active cycle times.

2.5.1. Active Cycle Times. According to the characteristics of the FDG active phase, three consecutive active cycle times (corresponding to the solids transports described by steps 1−3 of section 2.2) are identified:

(a). Active time of AS1 ($t_{i_{\mathrm{A1}}}$). At each discharging angular position, $t_{i_{\mathrm{A1}}}$ accounts for the time required by the solids to travel from the flight to the fluidization table. Figure 9 shows the AS1 fall height for a given angular position θ_i. Using the fall point (flight tip), the initial solids velocity, and the coordinates of the slope of the fluidized-table surface, the equations of motion are solved to finally calculate the average fall time.

The geometry and location of the fluidization table within the drum are presented in Figure 10. For melt granulation, air is blown from a central pipe through a flat perforated plate (see

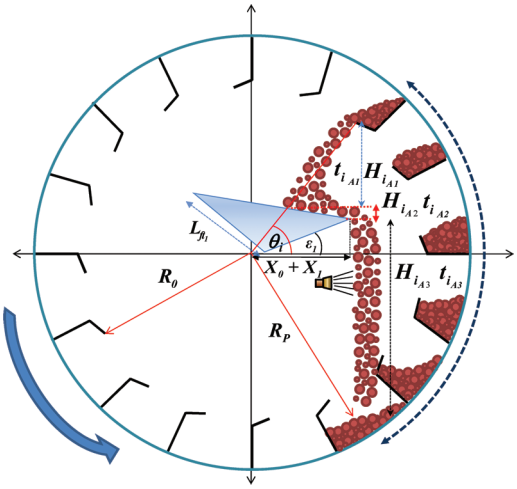

Figure 9. Geometrical parameters to calculate the active and passive cycle times.

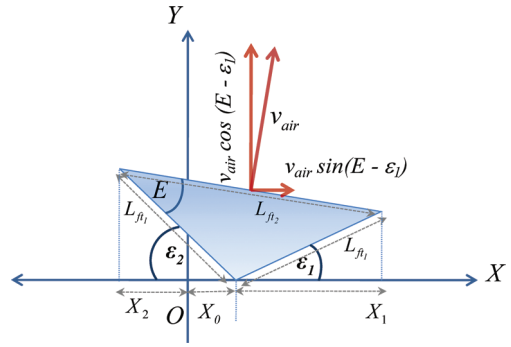

Figure 10. Fluidization table location and air velocity decomposition in the stationary coordinate system.

Figure 1) to cool down the granules. Therefore, the air is supposed to leave the fluidization table in a direction perpendicular to its surface (external fans draw the air out of the granulator).

A force balance for a particle located on the fluidization table, assuming that the buoyancy due to air is negligible and that there are spherical granules, gives

$$\frac{dv_Y}{dt} = -g\cos(\alpha_d) + \frac{3\rho_{air}C_D}{4d_p\rho_p}[v_{air}\cos(E - \varepsilon_1) - v_Y]^2 \quad (14)$$

$$\frac{dv_X}{dt} = \frac{3\rho_{air}C_D}{4d_p\rho_p}[v_{air}\sin(E - \varepsilon_1) - v_X]^2 \quad (15)$$

where C_D is the drag coefficient; ρ_{air} and ρ_p are the air and particle densities, respectively; and d_p is the volume mean particle diameter. C_D is calculated by means of the correlation given by Sherritt et al.,[26] later used by Britton et al.[17]

To solve eqs 14 and 15, the departure velocity of the particle from the flight is needed. This velocity is calculated accounting for the particle rolling on the solids surface contained in the flight and the influence of the drum angular velocity.[14] To estimate the rolling velocity, a new coordinate system is employed (x', y'; see Figure 11a). By means of a force balance, the rolling velocity becomes

$$v_{ix'} = (2L_ig\cos(\alpha_d)[\sin(\phi_i) - \mu\cos(\phi_i)])^{1/2} \quad (16)$$

Figure 11b shows the tangential velocity in terms of the stationary coordinate system. In view of this contribution and the rolling velocity (eq 16) expressed in terms of the system (X, Y), the particle departure velocity can be expressed as

$$v_{iX}^0 = -\omega R_0\sin(\theta_i) - (2L_ig\cos(\alpha_d)[\sin(\phi_i) - \mu\cos(\phi_i)])^{1/2}\cos(\phi_i) \quad (17)$$

$$v_{iY}^0 = \omega R_0\cos(\theta_i) - (2L_ig\cos(\alpha_d)[\sin(\phi_i) - \mu\cos(\phi_i)])^{1/2}\sin(\phi_i) \quad (18)$$

Using eqs 17 and 18 and considering that, for $t = 0$, a certain particle is located at the position given by $Y^0 = R_0\sin(\theta_i)$ and $X^0 = R_0\cos(\theta_i)$, eqs 14 and 15 can be integrated twice to obtain the position of a granule above the fluidization table as a function of time. The active time $t_{i_{A1}}$ is established for the condition of intersection between the particles trajectory and the equation that represents the location of the fluidization table surface, which for a cross-sectional area corresponding to an isosceles triangle is given by (see Figure 10)

$$Y = L_{f,t_1}\sin\varepsilon_1 - \frac{\sin(\varepsilon_2) - \sin(\varepsilon_1)}{\cos(\varepsilon_2) + \cos(\varepsilon_1)}[X - X_0 - L_{f,t_1}\cos(\varepsilon_1)] \quad (19)$$

(b). Active time of AS2 ($t_{i_{A2}}$). As was mentioned, because of the fluidization-table inclination, the particles roll down along its surface. The time associated with this transport is a function of the location on the fluidization table where the particles reach its surface; this contact point is also dependent on the discharging angular position. In fact, the distance traveled by the particles along the table increases with θ_i (see Figure 9).

The particle rolling velocity on the table is calculated by means of a force balance at the fluidization-table surface, as illustrated in Figure 12a. Considering another coordinate system (x'', y'') and assuming that, for $t = 0$, a certain particle is located on the table surface at $x'' = 0$ with zero velocity ($v_{ix''}^0 = 0$), the equation of particle motion (which considers the friction force on the aerated table surface to be negligible) is integrated twice to obtain the distance traveled by the rolling particle as a function of time:[11]

$$x'' = g\cos(\alpha_d)\sin(E - \varepsilon_1)\frac{t^2}{2} \quad (20)$$

The active time $t_{i_{A2}}$ is evaluated from eq 20 for the particles that reach the fluidization table edge (x''_e, see Figure 12b); the corresponding traveled vertical distance is

$$H_{i_{A2}} = x''_e\sin(E - \varepsilon_1) \quad (21)$$

(c). Active time of AS3 ($t_{i_{A3}}$). As is illustrated in Figure 9, $t_{i_{A3}}$ is the time required by a falling particle to travel from the fluidization table edge to the mean radius (R_p), defined by Britton et al.[17] as follows:

$$R_p = \frac{(R + R_0)}{2} \quad (22)$$

The particle rolling velocity at the table edge represents the initial velocity ($v_{ft,ti}^0$) of the particles that fall from the fluidization table toward the spray zone:

$$v_{ft_i}^0 = -[2x''_{e_i}g\cos(\alpha_d)\sin(E - \varepsilon_1)]^{1/2} \quad (23)$$

$v_{ft_i}^0$ corresponds to the initial velocity in the x'' direction; its decomposition in the (X, Y) system becomes

$$v^0_{\mathrm{ft}_i Y} = -[2x''_{\mathrm{e}_i} g\cos(\alpha_\mathrm{d})\sin(E-\varepsilon_1)]^{1/2}\sin(E-\varepsilon_1) \quad (24)$$

$$v^0_{\mathrm{ft}_i X} = -[2x''_{\mathrm{e}_i} g\cos(\alpha_\mathrm{d})\sin(E-\varepsilon_1)]^{1/2}\cos(E-\varepsilon_1) \quad (25)$$

Assuming that the particles that drop from the table edge follow a parabolic free-fall trajectory, the traveled distances from the initial position X^0_P, Y^0_P (see Figure 12b) are given by

$$X_\mathrm{P} = X^0_\mathrm{P} + v^0_{\mathrm{ft}_i X}t = X_0 + L_{\mathrm{ft}1}\cos(\varepsilon_1) + v^0_{\mathrm{ft}_i X}t \quad (26)$$

$$Y_\mathrm{P} = Y^0_\mathrm{P} + v^0_{\mathrm{ft}_i Y}t - \frac{1}{2}gt^2 = L_{\mathrm{ft}1}\sin(\varepsilon_1) + v^0_{\mathrm{ft}_i Y}t - \frac{1}{2}gt^2 \quad (27)$$

The active time $t_{i_{\mathrm{A}3}}$ and the distance $H_{i_{\mathrm{A}3}}$ (Figure 9) are calculated by intersecting the trajectory defined by eqs 26 and 27 with the equation of a circumference of radius R_P.

2.5.2. Passive Cycle Times. The passive time t^i_P is defined as the time the particle takes to travel within the drum from the reentry point (at the bottom of the unit) to its original flight discharge angular position θ_i. As proposed by Britton et al.[17] and based on the geometry described by Figure 9, the passive time becomes

$$t_{i_\mathrm{p}} = \frac{1}{\omega}\left[\theta_i + \cos^{-1}\left(\frac{X^*_\mathrm{P}}{R_\mathrm{P}}\right)\right] \quad (28)$$

where X^*_P denotes the X coordinate of the particle's reentry point.

2.5.3. Mass-Average Cycle Times. The mass-average active and passive cycle times are obtained by adapting the guidelines proposed by Britton et al.[17] to the FDG active-phase characteristics. These average times, which take into account the active and passive times at each angular position weighted by the mass flow rates of each subcell, are

$$\bar{t}^j_{i_{\mathrm{A}1}} = \frac{\sum_i \dot{m}^j_{i_{\mathrm{A}1}} t_{i_{\mathrm{A}1}}}{\sum_i \dot{m}^j_{i_{\mathrm{A}1}}} \quad (29)$$

$$\bar{t}^j_{i_{\mathrm{A}2}} = \frac{\sum_i \dot{m}^j_{i_{\mathrm{A}2}} t_{i_{\mathrm{A}2}}}{\sum_i \dot{m}^j_{i_{\mathrm{A}2}}} \quad (30)$$

$$\bar{t}^j_{i_{\mathrm{A}3}} = \frac{\sum_i \dot{m}^j_{i_{\mathrm{A}3}} t_{i_{\mathrm{A}3}}}{\sum_i \dot{m}^j_{i_{\mathrm{A}3}}} \quad (31)$$

where the mass flows between the active zones are defined as

$$\dot{m}^j_{i_{\mathrm{A}2}} = (1 - C^j_{\mathrm{f}_{\mathrm{A}1}})\dot{m}^j_{i_{\mathrm{A}1}} + C^{j-1}_{\mathrm{f}_{\mathrm{A}1}}\dot{m}^{j-1}_{i_{\mathrm{A}1}} \quad (32)$$

$$\dot{m}^j_{i_{\mathrm{A}3}} = (1 - C^j_{\mathrm{f}_{\mathrm{A}2}})\dot{m}^j_{i_{\mathrm{A}2}} + C^{j-1}_{\mathrm{f}_{\mathrm{A}2}}\dot{m}^{j-1}_{i_{\mathrm{A}2}} + \dot{m}^j_{i_{\mathrm{melt}}} \quad (33)$$

Considering that all the melt droplets contribute to particle growth (i.e., the formation of nuclei by overspray and the loss of melt droplets by elutriation are neglected) and that the total melt is evenly distributed by the nozzles located equispaced along the drum, the melt flow rate in each cell can be calculated as follows:

$$\dot{m}^j_{\mathrm{melt}} = \frac{\dot{m}_{\mathrm{melt}}}{N_\mathrm{c}} \quad (34)$$

The particles that leave the flights reach the fluidization table at different points; for this reason, the parabolic trajectory from the table edge toward the spray zone depends on the discharge angle. The granules that fall from the flights at lower discharge

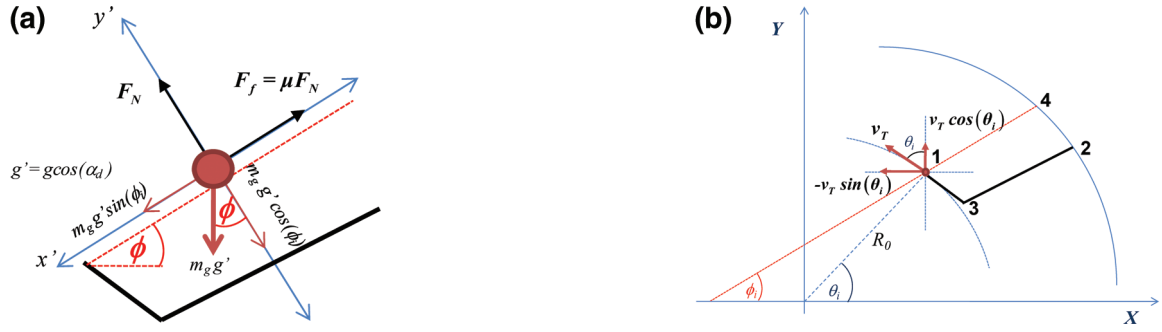

Figure 11. (a) Force balance for a rolling granule discharging from a flight and (b) particle departure velocity.

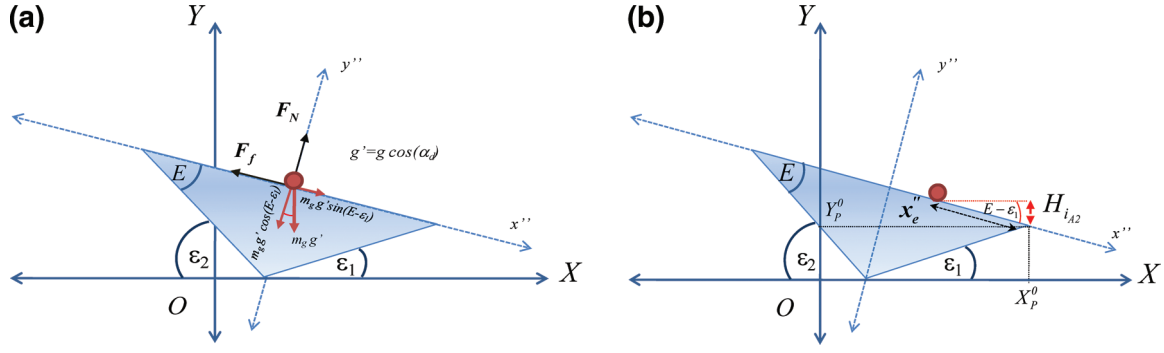

Figure 12. (a) Force balance for a rolling particle at the fluidization table surface. (b) Vertical distance traveled by a particle rolling down the fluidization table.

angles have more probability to be coated by the sprayed binder; therefore, the following equation is proposed to represent the melt distribution according to the particles' discharge angle:

$$\dot{m}^{j}_{i_{\mathrm{melt}}} = \dot{m}^{j}_{\mathrm{melt}}\left(\frac{\theta_{\mathrm{fin}} - \theta_i}{\theta_{\mathrm{fin}} - \theta_{\mathrm{in}}}\right) \tag{35}$$

where θ_{in} and θ_{fin} represent the initial and final discharge angle positions, respectively.

After the calculation of the mass-average times, the transport coefficients k^j_1 to k^j_4 are evaluated by means of the following equations:[17]

$$k^{j}_{1} = \frac{1}{\bar{t}^{j}_{i_{\mathrm{A1}}}} \tag{36}$$

$$k^{j}_{2} = \frac{1}{\bar{t}^{j}_{i_{\mathrm{A2}}}} \tag{37}$$

$$k^{j}_{3} = \frac{1}{\bar{t}^{j}_{i_{\mathrm{A3}}}} \tag{38}$$

$$k^{j}_{4} = \frac{1}{\bar{t}^{j}_{i_{\mathrm{p}}}} \tag{39}$$

The forward partitioning coefficients are determined as the ratio of the average forward migration of the falling solids in the corresponding active phase to the length selected for the cells:

$$C^{j}_{\mathrm{f}_{\mathrm{A1}}} = \frac{\bar{H}_{\mathrm{A1}}\sin(\alpha_{\mathrm{d}})}{L_{\mathrm{f}}/N_{\mathrm{c}}} = \left[\frac{\sum_i \dot{m}^{j}_{i_{\mathrm{A1}}} H_{i_{\mathrm{A1}}}}{\sum_i \dot{m}^{j}_{i_{\mathrm{A1}}}}\right]\frac{\sin(\alpha_{\mathrm{d}})}{L_{\mathrm{f}}/N_{\mathrm{c}}} \tag{40}$$

$$C^{j}_{\mathrm{f}_{\mathrm{A2}}} = \frac{\bar{H}_{\mathrm{A2}}\sin(\alpha_{\mathrm{d}})}{L_{\mathrm{f}}/N_{\mathrm{c}}} = \left[\frac{\sum_i \dot{m}^{j}_{i_{\mathrm{A2}}} H_{i_{\mathrm{A2}}}}{\sum_i \dot{m}^{j}_{i_{\mathrm{A2}}}}\right]\frac{\sin(\alpha_{\mathrm{d}})}{L_{\mathrm{f}}/N_{\mathrm{c}}} \tag{41}$$

$$C^{j}_{\mathrm{f}_{\mathrm{A3}}} = \frac{\bar{H}_{\mathrm{A3}}\sin(\alpha_{\mathrm{d}})}{L_{\mathrm{f}}/N_{\mathrm{c}}} = \left[\frac{\sum_i \dot{m}^{j}_{i_{\mathrm{A3}}} H_{i_{\mathrm{A3}}}}{\sum_i \dot{m}^{j}_{i_{\mathrm{A3}}}}\right]\frac{\sin(\alpha_{\mathrm{d}})}{L_{\mathrm{f}}/N_{\mathrm{c}}} \tag{42}$$

For an overloaded FDG, the kilning flow requires the evaluation of k^j_5, which is given by

$$k^{j}_{5} = \frac{\omega}{\theta^{j}_{k}} \tag{43}$$

The kilning angle (θ^j_k) can be established once the drum-passive mass is computed from eq 12. The equation to evaluate the kilning angle, reported by Britton et al.,[17] is

$$\frac{m^{j}_{\mathrm{p,drum}}}{L_{\mathrm{f}}\rho_{\mathrm{b}}} = \frac{R^2}{2}[\theta^{j}_{k} - \sin(\theta^{j}_{k})] \tag{44}$$

2.6. Steady-State Mass Balances for a FDG. 2.6.1. Passive Solids Mass Balance. Assuming that $\dot{m}^0_{\mathrm{s}}$ (recycle stream of the granulation circuit) enters into the FDG unit at the passive zone, the mass balance for cell 1 becomes (see Figure 6)

$$\dot{m}^{0}_{\mathrm{s}} + (1 - C^{1}_{\mathrm{f,A3}})k^{1}_{3}m^{1}_{\mathrm{a3}} - k^{1}_{5}m^{1}_{\mathrm{k}} - k^{1}_{4}m^{1}_{\mathrm{p}} = 0 \text{ for } j = 1 \tag{45}$$

For the subsequent cells, the mass balance is given by

$$k^{j-1}_{5}m^{j-1}_{\mathrm{k}} + C^{j-1}_{\mathrm{f,A3}}k^{j-1}_{3}m^{j-1}_{\mathrm{a3}} + (1 - C^{j}_{\mathrm{f,A3}})k^{j}_{3}m^{j}_{\mathrm{a3}} - k^{j}_{5}m^{j}_{\mathrm{k}} - k^{j}_{4}m^{j}_{\mathrm{p}} = 0 \tag{46}$$

where $C^{N_{\mathrm{c}}}_{\mathrm{f,A3}} = 0$.

2.6.2. Active Solids Mass Balances.

$$k^{j}_{4}m^{j}_{\mathrm{p}} - k^{j}_{1}m^{j}_{\mathrm{a1}} = 0 \tag{47}$$

$$C^{j-1}_{\mathrm{f,A1}}k^{j-1}_{1}m^{j-1}_{\mathrm{a1}} + (1 - C^{j}_{\mathrm{f,A1}})k^{j}_{1}m^{j}_{\mathrm{a1}} - k^{j}_{2}m^{j}_{\mathrm{a2}} = 0 \tag{48}$$

$$C^{j-1}_{\mathrm{f,A2}}k^{j-1}_{2}m^{j-1}_{\mathrm{a2}} + (1 - C^{j}_{\mathrm{f,A2}})k^{j}_{2}m^{j}_{\mathrm{a2}} + \dot{m}^{j}_{i_{\mathrm{melt}}} - k^{j}_{3}m^{j}_{\mathrm{a3}} = 0 \tag{49}$$

where $C^0_{\mathrm{f,A1}} = C^0_{\mathrm{f,A2}} = C^{N_{\mathrm{c}}}_{\mathrm{f,A1}} = C^{N_{\mathrm{c}}}_{\mathrm{f,A2}} = 0$. The mass balance given by eq 47 assumes negligible the particles elutriation above the fluidization bed.

3. FDG Operating and Geometrical Parameters

The features of a drum can vary greatly.[13] On the basis of the geometrical data reported by Degrève et al.[27] for a 26−30 TPH (tons per hour) NPK flighted drum granulator, a diameter of 4.3 m and equispaced perpendicular two-segment flights are selected for the FDG studied in this work. Considering the ratio $L_{\mathrm{d}}/D_{\mathrm{d}} = 2$ proposed by Capes[28] for fertilizer granulation drums, a length $L_{\mathrm{d}} = 8.6$ m is fixed. A flight segment l' (see Figure 7) of 0.07 m and a fold angle (α_{A}) equal to 135° are chosen. Because of the limited available information regarding the fluidized-table dimensions and location, the following parameters are specified (see Figure 10): $L_{\mathrm{f},t_2} = 1.75$ m, $L_{\mathrm{f},t_1} = 1.19$ m, eccentricity (X_0) = 0.45 m, right angle (ε_1) = 37°.[9] For a granulator output of about 14−16 kg/s (i.e., a 26−30 TPH plant capacity with a recycle ratio of 1:1),[9] a mean granule size enlargement of about 20−30% is attainable,[6] which is desired to obtain round granules. To ensure that all the granules fall from the flights onto the fluidized table surface, the flights number (N_{f}) and base segment length (l, see Figure 7) as well as the drum inclination and rotational speed have to be carefully selected. The values of these variables are established by trial and error to define a base case: $l = 0.24$ m, 20 flights, a drum slope of 5°, and a 5 rpm rotational speed. Except for the base segment length, the other mentioned variables are modified to study their effect on the solids flow patterns.

The air mass flow rate required for cooling purposes is determined by the melting point of the fertilizer and the plant capacity. Potassium nitrate is selected as model fertilizer (melting temperature = 333 °C). A total air mass flow rate of 25 kg s^{-1} is chosen in order to adiabatically cool down the output to 140−150 °C and thus to guarantee the β rhombohedral structure for the particles that leave the granulation unit.[8,29,30] All the geometrical and operating variables selected to define the base case are summarized in Table 1.

4. Numerical Solution

To solve the described FDG steady-state compartment model, the kinetic angle of repose, cross-sectional area, and cord length of the material contained in the flights are estimated for every angular position. This first calculation is required to determine the rotation angles for which the flight solids discharge begins and finishes and to estimate the mass flows ($\dot{m}^j_{i_{\mathrm{A1}}}$) of the solids

Table 1. FDG Base Case: Geometrical and Operating Variables

Drum Geometry	
D_d, m	4.3
L_d, m	8.6
α_d, (deg)	5
Flights Number and Geometry	
l', m	0.07
l, m	0.24
α_A, (deg)	135
L_f, m	8.6
N_f	20
Fluidization Table Geometry and Location	
X_0, m	0.45
L_{ft_1}, m	1.19
L_{ft_2}, m	1.75
ε_1, (deg)	37
Operating Variables	
$\dot{m}_s^0$, kg s^{-1}	8.3
$\dot{m}_{melt}$, kg s^{-1}	8.3
$\dot{m}_a$, kg s^{-1}	25
ω, rad s^{-1}	0.5234 (5 rpm)

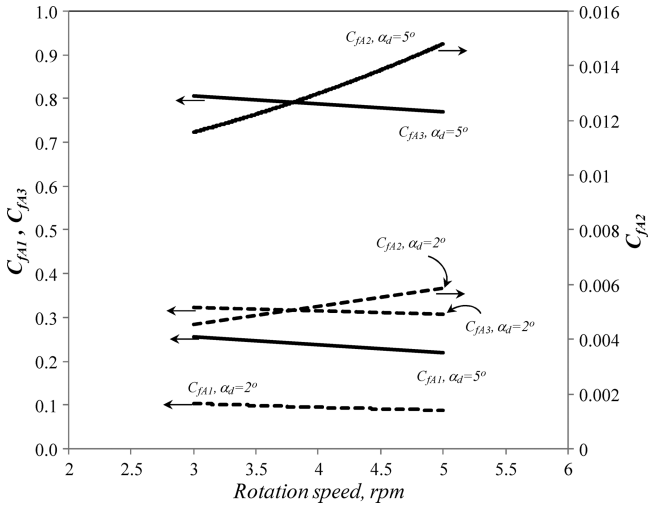

Figure 13. Forward partitioning coefficients as a function of α_d and rotation speed.

discharged from the flights as the drum rotates. The time and traveled distance for the three active subzones (AS1, AS2, and AS3) and the passive phase (PS) are then calculated. After computing the mass flow rate of the particles discharged by the flights at different rotation angles ($\dot{m}^j_{iA1}$), the mass-average cycle times, which allow for estimating the transport coefficients between the active and passive phases (k_1^j to k_4^j), are evaluated. The forward partitioning coefficients (C^j_{fA1} to C^j_{fA3}) are also computed. Assuming an underloaded operating regime, the steady-state mass balances are next solved. Subsequently, the passive solids mass is compared with the design load. If the drum load hypothesis is incorrect, the kilning transport coefficient (k_5^j) is estimated and the steady-state mass balances are solved again.

The described calculation procedure is repeated for a different fixed number of model cells (N_c) to assess the optimal number of compartments that can provide a good balance between the solution accuracy and the computing time. For the base case defined by Table 1, about 50 compartments are required to accurately represent the FDG (the mass error predictions are lower than 0.2%). Therefore, this discretization step is used for all the simulations performed in this work. The maximum number of cells, for which the maximum axial advance results equal to the cell length, is 65.[18]

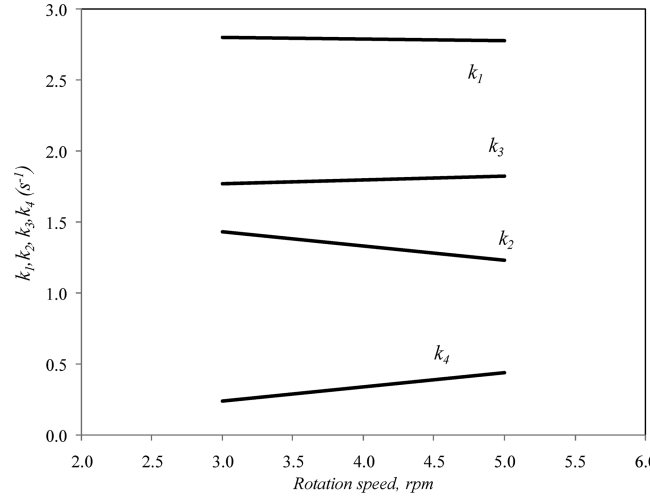

Figure 14. Solids transport coefficients as a function of the rotation speed ($\alpha_d = 5°$).

5. Results and Discussion

According to the developed model, the partitioning coefficients are constant for all the cells (except for cells 0 and N_c for which the partitioning coefficients are set equal to zero). Figure 13 shows the forward partitioning coefficients, for any cell, as a function of the rotational speed and the drum inclination angle (the other variables are fixed at the corresponding values listed in Table 1). The coefficients $C^j_{fA2}$and $C^j_{fA3}$are the lowest and highest ones, respectively, independent of the selected α_d and ω values. This result is in good agreement with the distances $\bar{H}_{A2}$ and $\bar{H}_{A3}$ traveled by the solids in the active zones 2 and 3 (see Figure 9).

For a given drum inclination angle, C^j_{fA1}decreases as the rotational speed is increased. This behavior is directly related with the effect of the drum angular velocity on the solids departure velocity from the flights (eqs 17 and 18): the higher the rotational speed, the higher is the initial solids velocity. As a result, the particles reach the fluidization table at shorter distances $\bar{H}_{A1}$, leading to less forward solids transport. For the same reason, as ω increases, longer are the distances $\bar{H}_{A2}$ traveled by the solids and higher C^j_{fA2} coefficients are expected. In addition and because of the greater x_e'' values, the result is that the initial particle velocities at the fluidization table edge (eqs 24 and 25) are higher. Consequently, the particles reach the drum walls within shorter distances $\bar{H}_{A3}$ and C^j_{fA3} decreases. For the FDG design of the base case, the minimum and maximum rotational speeds, to avoid the solids discharge from the flights outside of the fluidization table, are about 3 and 9 rpm, respectively.

As can be seen in Figure 13, as the drum inclination angle diminishes, the partitioning coefficients decrease. This effect is caused by the direct influence of α_d on these parameters (eqs 40−42). The diminution observed for all the partitioning coefficients is given basically by the relationship [sin(2°)/sin(5°)].

Figure 14 shows the solids transport coefficients as a function of the rotational speed, with the other variables being the ones listed in Table 1. Accordingly with the model assumptions, the transport coefficients k_1-k_4 are identical for all the cells (except for $j = 0$ and $j = N_c$) and are not affected by the number of flights. The solids transport coefficients are not significantly influenced by the inclination angle. In fact, for changes in the inclination angle from 5° to 2°, the transport coefficients exhibit differences lower than 0.3%.

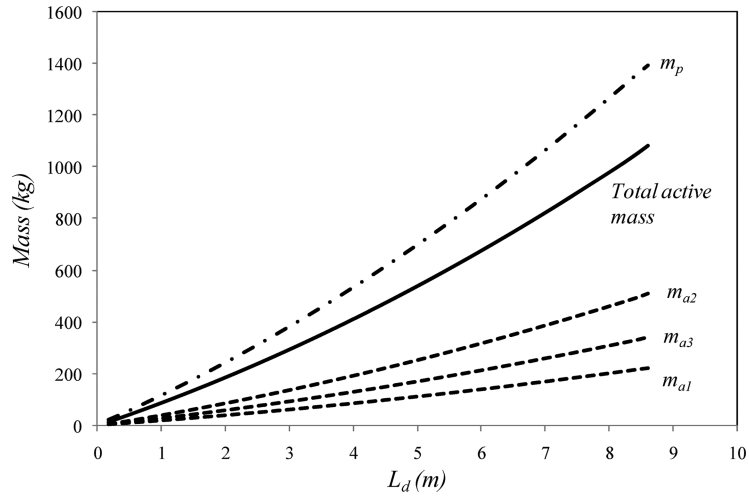

Figure 15. Cumulative active and passive mass holdups as a function of the drum length.

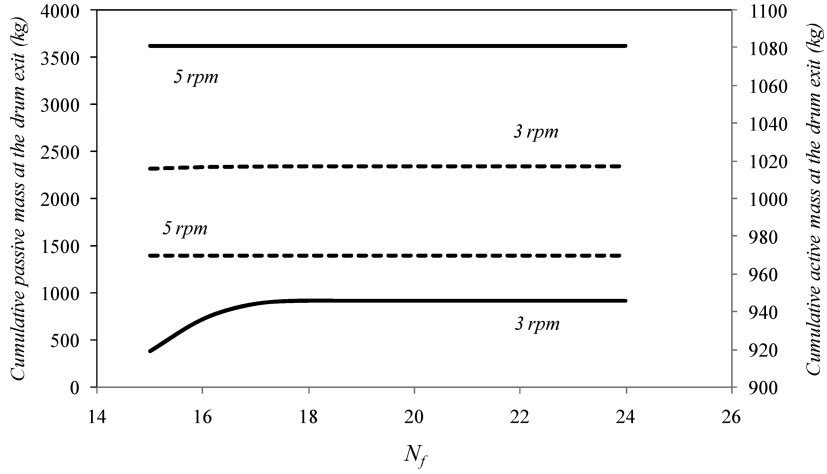

Figure 16. Cumulative active (solid lines) and passive (dashed lines) mass holdups at the drum exit for different rotational speeds and flights number ($\alpha_d = 5°$).

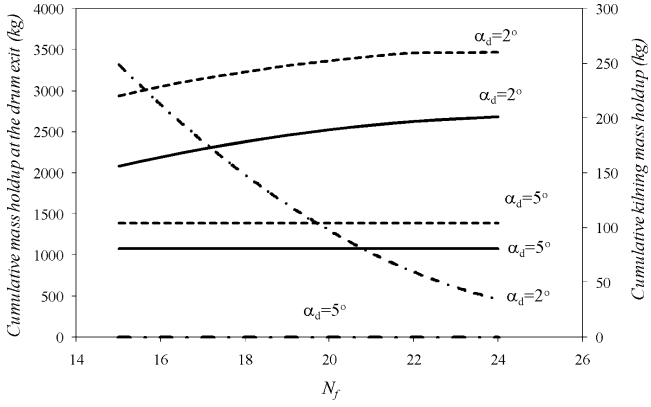

Figure 17. Cumulative active (solid lines), passive (dashed lines) and kilning (dot-dashed lines) mass holdups at the drum exit for different inclination angles and flights number. Rotational speed = 5 rpm.

The transport coefficient k_1 does not vary significantly against changes in the rotational speed. The higher the rotational speed, the higher is the solids departure velocity from the flights. However and despite the higher departure velocity, the particles travel longer distances along their parabolic trajectory before reaching the fluidization table. As ω increases, the location at which the particles intersect the table surface is also higher (x_e'', see Figure 12b). For this reason and considering eq 20, higher AS2 active times and, therefore, lower k_2 are obtained as the drum rotates faster. Regarding k_3, the higher ω, the higher is the solids initial velocity at the table edge and, thus, the shorter are the distances $\bar{H}_{A3}$. As a result, the active time of zone AS3 diminishes and consequently k_3 rises, as the drum rotation is increased. The passive cycle time is inversely proportional to the angular velocity (eq 31); therefore, as the drum rotation is increased, higher transport coefficients k_4 are observed.

For the base case defined in Table 1, the cumulative active and passive mass holdups as a function of the drum length are presented in Figure 15. The AS2 exhibits the highest mass holdup, basically because k_2 is the lowest solids transport coefficient of all the active zones. Almost 50% of the active mass holdup is concentrated on the table surface. The longer particles stay in this zone would contribute to satisfactorily meet the energy transfer required to cool down the granules and guarantee the later solidification of the melt droplets introduced in zone AS3. This result indicates that the fluidization table geometry has a great impact on the FDG performance, with these parameters being important design variables. Also and according to Figure 14, as the rotational speed is increased the lower is k_2 and, therefore, the higher is the AS2 mass holdup. The passive mass holdup is the highest one, in agreement with the values of k_4 that represents the lowest solids transport coefficient (Figure 14).

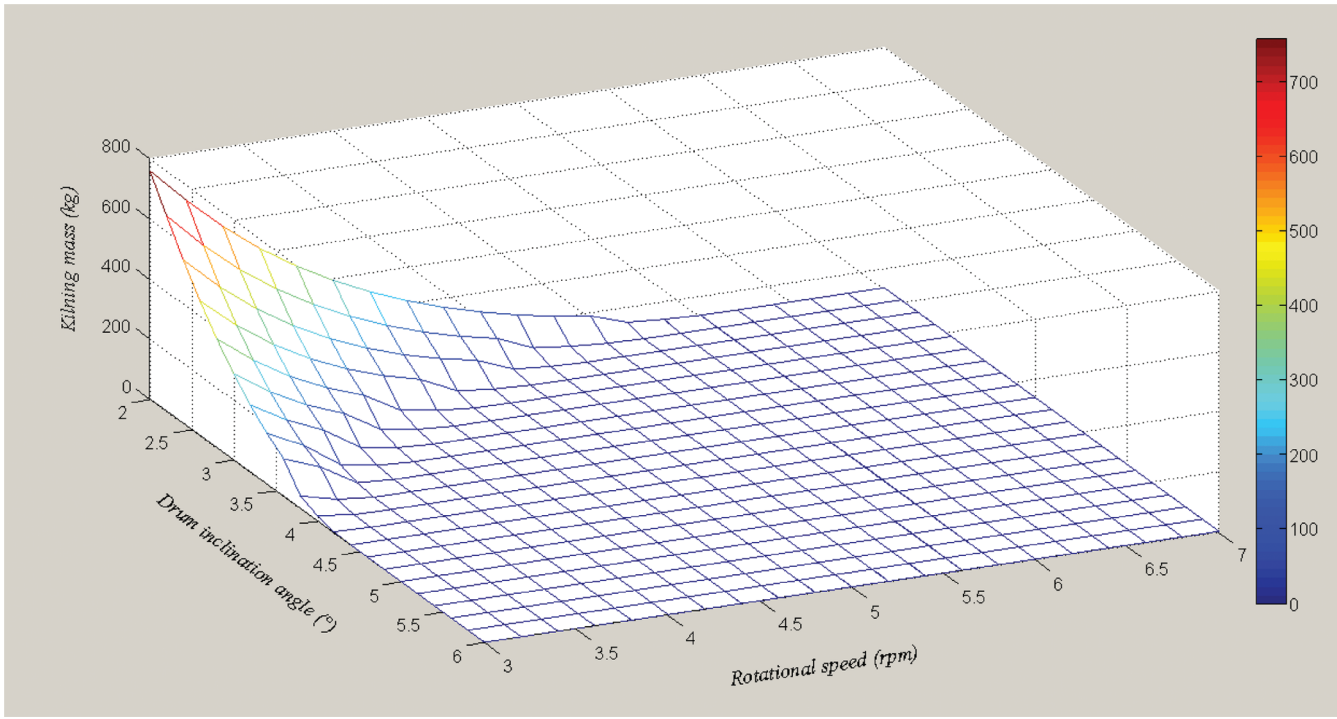

Figure 18. Kilning mass holdups at the drum exit for different inclination angles and rotational speeds ($N_f = 20$).

Figure 16 presents the cumulative total active and passive masses at the drum exit as a function of the flights number and drum rotational speed. As the angular velocity is raised, the passive and active mass holdups decrease and increase, respectively. This effect is in good agreement with the values of the solid transport coefficients presented in Figure 14. For example, if the rotational speed is increased from 3 to 5 rpm, the total active mass increases about 20% while the passive mass holdup decreases almost 40%. This result indicates that the rotational speed can be manipulated to govern the solids distribution within the drum and, consequently, to meet the energy requirements. At 5 rpm, the number of flights (between 15 and 24) does not affect the total mass holdups and the FDG operates at underloaded conditions. At 3 rpm, changes in the flights number may lead to kilning flow. As the angular velocity and the number of flights decrease, the flow of solids transported by the flights reaches the maximum allowable value given by eq 3. For this reason, kilning flow is observed in the system for 3 rpm and a number of flights lower than 17 (see eq 4).

The effect of the number of flights and the inclination angle on the mass holdups is shown in Figure 17. An inclination angle of 2° leads to active and passive mass holdups 1.9−2.5 and 2.1−2.5 times higher than the corresponding values for the base case. The inclination angle increment significantly diminishes the forward partitioning coefficients and, therefore, the solids migration toward the drum exit. For this reason, the mass holdups are greater. The kilning flow takes place at low inclination angles independently of the number of flights. Thus and according to the FDG operating features, the inclination angle cannot be strongly reduced. High flights number minimizes the kilning holdup, which is recommended to avoid an uneven particle growth.

6. Conclusions

The model presented in this work, which accounts for the solids mass flows and holdups in the different FDG zones, provides a firm foundation for integration with energy and population balances. The simultaneous solution of all the constitutive equations will allow improving the understanding of this unit and introducing design improvements to enhance the granules quality. The inclusion of energy and population balances will be the subject of future papers.

The fluidization table geometry and the angular velocity strongly affect the residence time of the particles on the fluidization table, resulting in them being variables that can be adjusted to meet the thermal requirements for the melt droplets solidification.

The passive mass holdup is the highest one in the FDG system. This result indicates that the energy transfer above the fluidization table has to be efficient to cool down the granules and to guarantee that all the particles are in the solid state before they are transported by the flights; otherwise, caking or agglomeration mechanisms may take place.

The rotational speed and inclination drum angle also appear as key variables since their values govern the solids distribution within the drum. Increments in the angular velocity increase the active mass holdup and reduce the passive mass. When the inclination angle is raised, both the active and passive mass holdups decrease. The number of flights has a strong influence on the kilning mass; if a diminution in this holdup is desired, relatively high drum inclination angles, rotational speeds, and number of flights should be used.

Nomenclature

C_D = drag coefficient (dimensionless)
C_f = forward partitioning coefficient (dimensionless)
d_p = particle volume mean diameter (m)
D = diameter (m)
E = fluidization table internal angle, see Figure 10 (radians)
F_f = friction force (N)
F_N = normal force (N)
g = acceleration due to gravity ($m^2\ s^{-1}$)
H = height (m)

k = solids transport coefficient (s^{-1})
L = length (m)
l' = length of the flight segment nearest to the tip (m)
l = base length of a flight (m)
m = mass holdup (kg)
m_g = granule mass (kg)
$\dot{m}$ = mass flow rate (kg s^{-1})
$\dot{m}_s^0$ = recycle stream of a granulation circuit (kg s^{-1})
N_c = number of compartments selected for the cell model (dimensionless)
N_f = total flights number (dimensionless)
R = drum radius (m)
R_0 = distance from the flight tip to the center of the drum (m)
R_P = mean radius, see eq 22 (m)
S = flight cross-sectional area filled with solids (m^2)
t = time (s)
v_{air} = air velocity (m s^{-1})
v_Y = particle velocity in the Y coordinate direction (m s^{-1})
v_X = particle velocity in the X coordinate direction (m s^{-1})
$v_{x'}$ = maximum initial velocity of a single particle falling from a flight (m s^{-1})
v_T = tangential velocity (m s^{-1})
X = stationary horizontal axis (m)
x = abscissa of the moving coordinate system (m)
Y = stationary vertical axis (m)
y = ordinate of the moving coordinate system (m)

Greek Letters

α_A = angle between the two flight segments (radians)
α_d = drum inclination angle (radians)
β = angle defined by eq 8 (radians)
δ = angle between the fixed and moving coordinate systems; this angle shown in Figure 7 is negative (radians)
$\gamma = \phi - \delta$ (radians)
ϕ = kinetic angle of repose (radians)
θ = angle of rotation (radians)
μ = dynamic coefficient of friction (dimensionless)
ω = angular velocity (radians s^{-1})
ρ = density (kg m^{-3})
ε_1 = right inclination angle of the fluidization table (radians)
ε_2 = left inclination angle of the fluidization table (radians)

Subscripts

air = air used as cooling medium in the fluidization table
A1 = active solids phase 1
A2 = active solids phase 2
A3 = active solids phase 3
b = bulk
d = drum
e = right fluidization table edge
f = flight
ft = fluidization table
i = angular position
k = kilning phase
melt = molten fertilizer used as binder
p = passive phase
1 = active mass phase 1
2 = active mass phase 2
3 = active mass phase 3
4 = passive mass
5 = kilning mass

Superscripts

0 = at $t = 0$
j = cell number

Literature Cited

(1) Barbosa-Cánovas, G. V.; Ortega-Rivas, E.; Juliano, P.; Yan, H. *Food Powders. Physical Properties, Processing and Functionality*; Kluwer Academic/Plenum Publishers: New York, 2005.

(2) Liu, L. X.; Litster, J. D. Population Balance Modeling of Granulation with a Physically Based Coalescence Kernel. *Chem. Eng. Sci.* **2002**, *57*, 2183–2191.

(3) Tan, H. S.; Goldschmidt, M. J. V.; Boerefijn, R.; Hounslow, M. J.; Salman, A. D.; Kuipers, J. A. M. Population Balance Modelling of Fluidized Bed Melt Granulation, An Overview. *Chem. Eng. Res. Des.* **2005**, *83*, 871–880.

(4) Saleh, K.; Guigon, P. Coating and encapsulation processes in powder technology. In *Handbook of Powder Technology*; Salman, A. D., Hounslow, M. J., Seville, J. P. K., Eds.; Elsevier: Amsterdam, The Netherlands, 2007.

(5) Valkov, S. Fluidized-bed granulation of ammonium nitrate and calcium−ammoniun nitrate. *Chem. Pet. Eng.* **2000**, *36*, 3–5.

(6) Thuring, P.; Vogel, E. The fluidized drum granulation process (FDG) and its various applications. Presented at IFA Technical Conference, Tunisia, 1986.

(7) Lauchard, D.; Kordek, M. Granulation KT's progress using fluidized drum granulation (FDG) technology. Presented at IFA Technical Conference, USA, 2000.

(8) Kaltenbach-Thuring. Fluid drum granulation of potassium nitrate. Nitrogen & Methanol, 1999, *237*, 53−55.

(9) Thuring, P.; Sombret, J.; Vogel, E. U.S. Patent 4,749,349, 1988.

(10) Kordek M. A. Granulation par pulverization de multiples couches minces de sels fondus dans un tambour a lit fluidise. Ph.D. Thesis, Université de Technologie de Compiègne, France, 1995.

(11) Litster, J. D.; Sarwono, R. Fluidized drum granulation of agglomerate formation. *Powder Technol.* **1996**, *88*, 165–172.

(12) Kelly, J. K. Flight design in rotary dryers. *Powder Technol.* **1992**, *10*, 979–993.

(13) Sherritt, R.; Caple, R.; Behie, L.; Mehrotra, A. The movement of solids through flighted rotating drums. Part I: Model formulation. *Can. J. Chem. Eng.* **1993**, *71*, 337–346.

(14) Wang, F. Y.; Cameron, I. T.; Litster, J. D.; Rudolph, V. A fundamental study of particle transport through rotary dryers for flight design and system optimization. *Drying Technol.* **1995**, *13*, 1261–1278.

(15) Revol, D.; Briens, C. L.; Chabagno, J. M. The design of flights in rotary dryers. *Powder Technol.* **2001**, *121*, 230–238.

(16) Sheehan, M. E.; Britton, P. F.; Schneider, P. A. A model for solids transport in flighted rotary dryers based on physical considerations. *Chem. Eng. Sci.* **2005**, *60*, 4171–4182.

(17) Britton, P. F.; Sheehan, M. E.; Schneider, P. A. A physical description of solids transport in flighted rotary dryers. *Powder Technol.* **2006**, *165*, 153–160.

(18) Lee, A. Modeling the solids transport phenomena within flighted rotary dryers. Ph.D. Thesis, James Cook University, Australia, 2008.

(19) Matchett, A. J.; Sheikh, M. S. An improved model of particle motion in cascading rotary dryers. *Trans. Inst. Chem. Eng.* **1990**, *68*, 139–148.

(20) Porter, S. J. The design of rotary driers and coolers. *Trans. Inst. Chem. Eng.* **1963**, *41*, 272–280.

(21) Lisboa, M. H.; Vitorino, D. S.; Delaiba, W. B.; Finzer, J. R. D.; Barrozo, M. A. S. A study of particle motion in rotary drier. *Braz. J. Chem. Eng.* **2007**, *24* (3), 365–374.

(22) Schofield, F. R.; Glikin, P. G. Rotary driers and coolers for granular fertilizers. *Trans. Inst. Chem. Eng.* **1962**, *40*, 183–189.

(23) Aphale, A.; Bolander, N.; Park, J.; Shaw, L.; Svec, J.; Wassgren, C. Granular fertiliser particle dynamics on and off a spinner spreader. *Biosyst. Eng.* **2003**, *85*, 319–329.

(24) Grift, T. E.; Kweon, G.; Hofstee, J. W.; Piron, E.; Villette, S. Dynamic friction coefficient measurement of granular fertilizer particles. *Biosyst. Eng.* **2006**, *95*, 507–515.

(25) Kweon, G.; Grift, T. E.; Miclet, D. A spinning-tube device for dynamic friction coefficient measurement of granular fertilizer particles. *Biosyst. Eng.* **2007**, *97*, 145–152.

(26) Sherritt, R. G.; Caple, R.; Behie, L. A.; Mehrotra, A. K. The movement of solids through flighted rotating drums. 2. Solids gas interactions and model validation. *Can. J. Chem. Eng.* **1994**, *72*, 240–248.

(27) Degrève, J.; Baeyens, J.; Van de Velden, M. Spray-agglomeration of NPK-fertilizer in a rotating drum granulator. *Powder Technol.* **2006**, *163*, 188–195.

(28) Capes C. E. *Handbook of Powder Technology; Vol 1: Particle Size Enlargement*; Elsevier Science: Amsterdam, The Netherlands, 1980.

(29) Westphal, M. J.; Wood, J. W.; Redin, R. D.; Ashworth, T. Calorimetric and photoacoustic investigation of KNO_3 phase transitions. *J. Appl. Phys.* **1993**, *73* (11), 7302–7310.

(30) Kumar, N.; Nath, R. Thermal and ferroelectric properties of potassium nitrate: Polyvinylidene fluoride composite films. *IEEE Trans. Dielectr. Electr. Insul.* **2005**, *12* (6), 1145–1150.

Received for review October 28, 2009
Revised manuscript received December 15, 2009
Accepted December 21, 2009

IE901691V